

Model-Free Stochastic Process Modeling and Optimization using Normalizing Flows

Eike Cramer^{a,*} 

^a RWTH Aachen University, Process Systems Engineering (AVT.SVT), Aachen 52074, Germany

Abstract: Real-world chemical processes often exhibit stochastic dynamics with non-trivial correlations and state-dependent fluctuations. However, most process models simply add stationary noise terms to a deterministic prediction, which can lead to inaccurate predictions. This work proposes using conditional normalizing flows as discrete-time models (DTMs) to learn the stochastic dynamics of chemical processes. Normalizing flows learn an explicit expression of the system states' probability density function (PDF) given prior states and control inputs. The resulting model naturally allows for formulating stochastic and probabilistic setpoint-tracking objectives and chance constraints. In applications to a continuous reactor and a reactor cascade, the normalizing flow yields stable simulations over long time horizons and high-quality results in stochastic and probabilistic MPC formulation for open-loop control. Furthermore, a chance-constrained optimization finds reliable startup controls for the reactor cascade with stochastic reactions. In conclusion, the conditional normalizing flow presents an excellent choice for modeling nonlinear stochastic dynamics.

Keywords: Probabilistic regression; Model-free conditional probability distribution learning; Maximum Likelihood control; Chance-constrained dynamic optimization;

1 Introduction

Discrete-time models (DTMs) (Söderström, 2002) are well-established process models for dynamical systems and often provide the basis for modern control schemes such as model predictive control (MPC) (Rawlings et al., 2017). In their standard form, DTMs predict the system states at the time step $\mathbf{x}[k+1]$ as a function f of the states $\mathbf{x}[k]$ and the control inputs $\mathbf{u}[k]$ at the k -th time step:

$$\mathbf{x}[k+1] = f(\mathbf{x}[k], \mathbf{u}[k]) \quad (1)$$

Typically, DTMs are estimated from process data, and thus, the classic statistical models are some of the earliest adoptions of machine learning in chemical engineering (Söderström, 2002). Recently, machine learning models such as artificial neural networks (ANN) have become popular choices of DTMs with extensions to Lipschitz ANNs (Tan and Wu, 2024), physics-informed ANN (Zheng et al., 2023), and hybrid models (Wu et al., 2020). For a review of neural networks-based process models for MPC, the reader is referred to Ren et al. (2022).

Real-world process data often exhibits noise, e.g., form measurement noise or disturbances. Furthermore, some processes are stochastic in nature, i.e., they exhibit inherent stochastic dynamics (Mesbah et al., 2022). This stochastic behavior requires specialized modeling tools that describe the stochas-

tic dynamics of the process (Varshney et al., 2022). Still, most works using DTMs rely on deterministic modeling, i.e., the fitted models predict only the most likely realization of the systems states. Meanwhile, stochastic process models can learn and predict the dynamics of inherently stochastic processes and quantify the impact of measurement noise on the prediction. Using stochastic process models, MPC can be extended to stochastic MPC, which finds optimal controls under uncertainty (Mesbah, 2016). In a scenario-based stochastic MPC, the stochastic process model is evaluated multiple times to create scenarios of possible realizations. These scenarios are then used to formulate a stochastic program (Birge and Louveaux, 2011) that minimizes the empirical mean of the control deviation while maintaining feasibility for all scenarios. Similarly, stochastic MPC can also be formulated using chance constraints that ensure feasible control actions with a set probability (Schwarm and Nikolaou, 1999; Paulson et al., 2017).

Most established stochastic process models use an additive noise term, i.e., they describe the stochastic behavior by adding a state-independent zero-mean noise term to a deterministic prediction (Box et al., 1967; Mesbah, 2016). This approach neglects potential correlations between the noise in the different system states and can only account for a limited range of probability distributions. Further-

*E. Cramer, RWTH Aachen University, Process Systems Engineering (AVT.SVT), Aachen 52074, Germany
E-mail: eike.cramer@alumni.tu-berlin.de

more, the additive noise assumption is independent of the system's states, excluding any correlation between the system's states and the stochasticity. For fermentation processes, for instance, the noise intensity varies with the cell concentration [Álvarez et al. \(2018\)](#). Thus, there is a need for stochastic process models, e.g., in a DTM format, that can describe complex system behaviors, including nonlinear stochastic behavior with non-Gaussian distributions and state-dependent stochastic dynamics.

This work uses the deep generative model called normalizing flows ([Papamakarios et al., 2021](#)) as probabilistic DTM. Normalizing flows are flexible probability distribution models for multivariate random variables that learn explicit expressions of the probability density function (PDF) using invertible neural networks (INNs) ([Papamakarios et al., 2021](#)). The basic concept of normalizing flows can be extended to learn conditional PDFs by augmenting the INN with external inputs. Thus, normalizing flows also function as multivariate regression models for random variables ([Winkler et al., 2019; Rasul et al., 2021; Cramer et al., 2022b](#)), i.e., normalizing flows can be used as DTMs for multivariate dynamics of systems with correlated, non-Gaussian, and state-dependent noise. Notably, normalizing flows learn high-dimensional conditional PDFs without prior assumptions and, thus, provide a highly flexible modeling architecture for stochastic processes. The author has previously used normalizing flows for scenario generation of power generation time series ([Cramer et al., 2022a,b](#)) and electricity prices ([Cramer et al., 2023; Hilger et al., 2024](#)). The most common use case for normalizing flows is image generation ([Dinh et al., 2015, 2017; Grathwohl et al., 2018](#)).

Normalizing flow-based DTMs sample scenarios of process realizations that can be used to solve stochastic MPC problems. Furthermore, this work shows that the explicit expression for the conditional PDF of the system states can be used to formulate a probabilistic setpoint-tracking objective. This probabilistic objective represents a likelihood maximization for the controller, i.e., the optimizer maximizes the likelihood that the control inputs achieve the desired setpoints. Besides the setpoint-tracking objectives, normalizing flows naturally support formulating chance constraints for any inequality constraints on the process.

The remainder of this work is organized as follows: Section 2 reviews the basic concept of normalizing flows and presents how normalizing flows can be applied as process models. Section 3 shows

the stochastic MPC formulation and introduces the probabilistic MPC formulation using the explicit PDF expression learned using the normalizing flow. Furthermore, the section shows how to formulate chance constraints from normalizing flow-based system simulations. Section 4 applies the normalizing flow to learn the stochastic dynamics of a continuous stirred tank reactor (CSTR). The section also presents a simulation using the normalizing flow DTM and compares open-loop MPC results for the stochastic MPC, the probabilistic MPC, and a benchmark using the nominal model equations. Section 5 applies the normalizing flow DTM to optimize a startup schedule for a reactor cascade via chance-constrained formulations. Finally, Section 6 concludes this work.

2 Probabilistic regression using normalizing flows

This section introduces the general concept of conditional density estimation using normalizing flows and describes how normalizing flows can be used as probabilistic regression models.

2.1 Conditional density estimation using invertible neural networks

Normalizing flows are explicit multivariate probability distribution models, i.e., they provide an explicit expression for the PDF $p_X(\mathbf{x})$ of a multivariate random variable X ([Papamakarios et al., 2021](#)). By including external features, normalizing flows can also describe conditional PDFs $p_{X|Y}(\mathbf{x}|\mathbf{y})$ given given the external feature random variable Y ([Winkler et al., 2019; Cramer et al., 2022b](#)). The random variable X is described as a diffeomorphism of a standard Gaussian $Z \sim \phi(\mathbf{z})$, i.e., a bijective transformation where both forward and inverse are differentiable. Here, the ϕ is the standard Gaussian PDF, and Z must have the same dimensionality as X . In practice, the diffeomorphism is implemented as an INN $\mathbf{x} = T(\mathbf{z})$ that maps from the Gaussian to the data space ([Dinh et al., 2017](#)). For conditional distributions, the INN is augmented with the conditional information as additional inputs ([Rasul et al., 2021; Cramer et al., 2022b](#)):

$$\mathbf{x} = T(\mathbf{z}, \mathbf{y}) \quad (2)$$

Here, \mathbf{x} are samples from the probability distribution the normalizing flow aims to learn, i.e., the data, \mathbf{z} are samples of the multivariate standard

Gaussian, and \mathbf{y} is the numerical conditional information. The inverse of the conditional diffeomorphism reads:

$$\mathbf{z} = T^{-1}(\mathbf{x}, \mathbf{y}) \quad (3)$$

As the diffeomorphism T describes a change of variables, the conditional PDF of the random variable X is given by the change of variables formula (Papamakarios et al., 2021):

$$p_{X|Y}(\mathbf{x}|\mathbf{y}) = \phi(T^{-1}(\mathbf{x}, \mathbf{y})) |\det \mathbf{J}_{T^{-1}}(\mathbf{x}, \mathbf{y})| \quad (4)$$

In Equation (4), $\mathbf{J}_{T^{-1}}$ is the Jacobian matrix of the inverse of T .

Equation (4) describes the likelihood that a data point \mathbf{x} is part of the probability distribution $p_{X|Y}$ given the conditional inputs \mathbf{y} . The log of Equation (4) can be used to formulate a log-likelihood maximization (Papamakarios et al., 2021):

$$\max_{\Theta} \log p_{X|Y}(\mathbf{x}|\mathbf{y}; \Theta) \quad (5)$$

Here, Θ are the parameters of the INN. The training then maximizes the likelihood that the inverse transformation T^{-1} maps the data to a standard Gaussian. Normalizing flows can learn the probability distribution of any multivariate continuous random variable, including multi-modal or heavily skewed PDFs (Papamakarios et al., 2021; Dinh et al., 2017). The training via likelihood maximization is statistically consistent and asymptotically efficient (Rossi, 2018). Hence, normalizing flows are guaranteed to estimate the correct PDF for an infinite sample size. After training, samples of the Gaussian can be transformed using the forward transformation to generate new data or scenarios.

During training, the Jacobian determinant in Equation (4) has to be computed in every iteration making the training prohibitively expensive for non-specialized INN transformations (Dinh et al., 2015, 2017). The most popular implementation of INNs is the real non-volume preserving transformation (RealNVP) (Dinh et al., 2017) that builds powerful transformations using compositions of partial transformations. These partial transformations are designed to yield triangular Jacobians for efficient determinant computation as the product of the diagonal entries. For details on the RealNVP architecture and implementation, the reader is referred to the original paper by Dinh et al. (Dinh et al., 2017), the review by Papamakarios et al. (Papamakarios et al., 2021), and the author's previous works on normalizing flows (Cramer et al., 2022a,b, 2023; Hilger et al., 2024). In the following, all

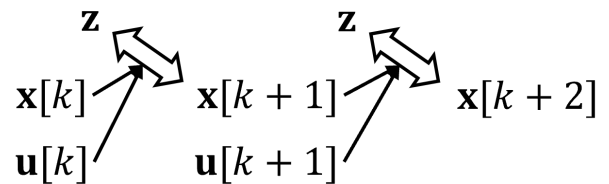


Fig. 1. Two steps of regression using normalizing flows. Here, $\mathbf{x}[k]$ are the states, $\mathbf{u}[k]$ are the control inputs, and $\mathbf{z} \sim \mathcal{N}(\mathbf{0}, \mathbb{I})$ is a multivariate Gaussian with $\dim(\mathbf{x}) = \dim(\mathbf{z})$. The two-headed arrow represents the INN with conditional inputs.

normalizing flows are implemented using RealNVP with the adaption to conditional random variables presented in Cramer et al. (2022b).

2.2 Probabilistic regression

The principle of training normalizing flows described in Section 2.1 translates to any combination of continuous uncertain variables X and conditional inputs Y . Thus, normalizing flows can be used as autoregressive models with exogenous inputs (AR-X). Similar to Equation (1), an AR-X models the next time step $\mathbf{x}[k+1]$ as a function of the previous time steps and the controls (Söderström, 2002). In the Markovian case, the functional relation is only built between the current time step $\mathbf{x}[k]$ and the control inputs $\mathbf{u}[k]$ at the given time t :

$$\mathbf{x}[k+1] = ARX(\mathbf{x}[k], \mathbf{u}[k]) + \epsilon \quad (6)$$

Here, $ARX(\cdot)$ is the autoregressive model, e.g., a statistical model (Box et al., 1967) or a neural network, and ϵ is an additive zero-mean noise term, which is usually set to be Gaussian. In the case of the normalizing flow regression model, the AR-X model in Equation (6) is substituted by the INN:

$$\mathbf{x}[k+1] = T_R \left(\mathbf{z}, \underbrace{[\mathbf{x}[k], \mathbf{u}[k]]}_{=\mathbf{y}} \right) \quad (7)$$

In Equation (7), T_R is the INN, and \mathbf{z} are samples of the standard Gaussian ϕ . Both the AR-X model in Equation (6) and the normalizing flow in Equation (7) sample different scenarios $\mathbf{x}_s[k+1]$ depending on the realizations ϵ_s and \mathbf{z}_s , respectively.

Figure 1 shows the regression scheme for two steps. Using the RealNVP model, i.e., the two-headed arrows in Figure 1, the transformation in Equation (7) is constructed to be diffeomorphic between the target variable $\mathbf{x}[k+1]$ and the Gaussian

variable \mathbf{z} . The previous states $\mathbf{x}[k]$ and the controls $\mathbf{u}[k]$ take the role of the conditional information \mathbf{y} in Equation (4). The inverse of (7) then reads:

$$\mathbf{z} = T_R^{-1}(\mathbf{x}[k+1], [\mathbf{x}[k], \mathbf{u}[k]]) \quad (8)$$

Note that RealNVP (Dinh et al., 2017) requires the number of states to be ≥ 2 but poses no limitations on the number of inputs \mathbf{u} , i.e., the inputs \mathbf{u} may be continuous or discrete.

The PDF of the predicted time step is again explicitly described via the change of variables formula:

$$\begin{aligned} p(\mathbf{x}[k+1] | [\mathbf{x}[k], \mathbf{u}[k]]) = \\ \phi(T_R^{-1}(\mathbf{x}[k+1], [\mathbf{x}[k], \mathbf{u}[k]))) \\ \cdot \left| \det \mathbf{J}_{T_R^{-1}}(\mathbf{x}[k+1], [\mathbf{x}[k], \mathbf{u}[k]]) \right| \end{aligned} \quad (9)$$

The normalizing flow-based regression model in Equation (7) samples scenarios $\mathbf{x}_s[k+1]$ from the probability distribution of possible realizations in Equation (9).

The probabilistic regression makes predicting multiple time steps nontrivial, as the predicted probability distribution from the first step must be propagated through the model to obtain the following steps. This work uses two approaches for this uncertainty propagation. The first approach computes the empirical mean $\bar{\mu}_{\mathbf{x}}[k+1]$ over these scenarios to be used as the inputs for the following time step. The second approach samples Monte Carlo samples, e.g., $N_s = 1000$, in the first time step and subsequently samples one scenario in every following time step for each scenario, respectively. The Monte Carlo samples then mimic a large number of particles that propagate through the stochastic transformations. The first approach is referred to as mean value propagation, and the second approach is referred to as Monte Carlo simulation.

For the mean value propagation, the empirical mean is given by:

$$\bar{\mu}_{\mathbf{x}}[k+1] = \frac{1}{N_s} \sum_{s=1}^{N_s} T_R(\mathbf{z}_s, [\mathbf{x}[k], \mathbf{u}[k]]) \quad (10)$$

Here, \mathbf{z}_s are samples of the Gaussian distribution that lead to the scenarios $\mathbf{x}_s[k+1]$. The next time step is given by:

$$\mathbf{x}[k+2] = T_R(\mathbf{z}, [\bar{\mu}_{\mathbf{x}}[k+1], \mathbf{u}[k+1]]) \quad (11)$$

The following time steps are computed analog to Equation (11).

The Monte Carlo simulation first samples N_s scenarios $\{\mathbf{x}[k+1]_s\}_{s \in 1, \dots, N_s}$ based on the initial state

$\mathbf{x}[k]$, where each scenario is sampled from the normalizing flow:

$$\mathbf{x}_s[k+1] = T_R(\mathbf{z}_s, [\mathbf{x}[k], \mathbf{u}[k]]) \quad (12)$$

Here, \mathbf{z}_s are randomly drawn samples from the multivariate Gaussian $\mathbf{z} \sim \phi$. For each scenario, a single sample is drawn for the following time step:

$$\mathbf{x}_s[k+2] = T_R(\mathbf{z}'_s, [\mathbf{x}_s[k+1], \mathbf{u}[k+1]]) \quad (13)$$

Here, \mathbf{z}'_s are new samples from the multivariate Gaussian. Over multiple time steps, the number of scenarios remains at N_s .

Sampling normalizing flows is efficient as each scenario requires a single feed-forward evaluation of the INN, i.e., Equation (7). Note that both propagation techniques result in N_s scenarios of the realization of the stochastic process. Normalizing flows allow for other types of uncertainty propagation. The author decided to restrict the evaluations in this work to the empirical mean propagation and the particle swarm simulation to limit the scope of this study.

3 Dynamic optimization using normalizing flows

This section discusses the two options for formulating stochastic and probabilistic state-tracking objectives using normalizing flows. First, Section 3.1 reviews the established formulation using the empirical mean-squared-error objective. Second, Section 3.2 introduces an objective based on the conditional log-likelihood described by the normalizing flow. Finally, Section 3.3 shows how chance constraints can be formulated from the normalizing flow predicted scenarios. All formulations in this section apply to either of the two approaches for multi-step predictions, i.e., the mean value propagation and the Monte Carlo simulation.

3.1 Stochastic objective

Setpoint MPC computes the controls \mathbf{u} by minimizing the predicted offset between the system setpoints \mathbf{x}^* and the controlled variables \mathbf{x} over the given time horizon $t = 1, \dots, N_T$, where N_T is the number of time steps. A stochastic model yields a distribution of system realizations and, thus, stochastic MPC minimizes the predicted expected offset between scenarios and setpoints (Mes-

bah, 2016):

$$\max_{\forall \mathbf{u}[k]} \sum_{k=0}^{N_T-1} \mathbb{E} \left[(\mathbf{x}^*[k+1] - \mathbf{x}[k+1])^2 \right] \quad (14)$$

Here, $\mathbf{x}[k+1]$ is the predicted value $\mathbf{x}[k+1](\mathbf{x}[k], \mathbf{u}[k])$. In practice, the objective in Equation (14) is implemented as the empirical mean over the considered scenarios.

$$\max_{\forall \mathbf{u}[k]} \sum_{k=0}^{N_T-1} \frac{1}{N_S} \sum_{s=1}^{N_S} (\mathbf{x}^*[k+1] - \mathbf{x}_s[k+1])^2 \quad (15)$$

Again, $\mathbf{x}_s[k+1]$ are the scenarios generated from the normalizing flow $\mathbf{x}_s[k+1](\mathbf{x}[k], \mathbf{u}[k])$. Evaluating the objective in Equation (15) over all time steps N_T requires $N_S \times N_T$ forward evaluations of the INN (Equation (7)), where the scenario evaluations N_S can be computed in parallel for each of the time steps.

3.2 Likelihood-based objectives

The normalizing flow-based regression model introduced in Section 2 gives an explicit expression for the conditional PDF that allows for the computation of the likelihood of the controls inducing the desired state values. Thus, this work investigates whether Equation (14) can be substituted with a log-likelihood maximization. For a single step $k \rightarrow k+1$, the maximum log-likelihood objective reads:

$$\max_{\mathbf{u}[k]} \log p(\mathbf{x}^*[k+1] | [\mathbf{x}[k], \mathbf{u}[k]]) \quad (16)$$

Here, $\mathbf{x}[k]$ are the current states, $\mathbf{u}[k]$ are the control inputs and degrees of freedom, $\mathbf{x}^*[k+1]$ are the setpoints for the next time steps, and $\log p(\cdot | \cdot)$ is the conditional log-likelihood function described by the change of variables formula in Equation (9). To extend the log-likelihood objective to a full horizon, the sum over the log-likelihoods of all time steps is maximized:

$$\max_{\forall \mathbf{u}[k]} \sum_{k=0}^{N_T-1} \log p(\mathbf{x}^*[k+1] | [\mathbf{x}[k], \mathbf{u}[k]]) \quad (17)$$

Optimizing the likelihood maximization in Equation (17) then maximizes the likelihood that the system converges to the setpoints for the probability distribution described by the normalizing flow and given the respective previous states and the control inputs.

Solving the optimization problem in Equation (17) requires $N_S \times N_T$ evaluations of the forward INN (Equation (7)) for either propagation approach. Like the stochastic formulation, the scenario evaluations can be computed in parallel for each time step. Additionally, computing the log-likelihood requires an additional inverse evaluation of the INN (Equation (8)), which can be computed in parallel for all time steps after computing all scenarios.

The explicit formulation of the conditional PDF in Equation 9 gives a single likelihood value for all states at a given time $\mathbf{x}[k+1]$. Thus, all modeled states must have a setpoint $\mathbf{x}^*[k+1]$ to make Equation (17) solvable.

3.3 Chance constraints

Normalizing flows model the joint probability distribution of all dynamic states $\mathbf{x}[k]$ at a given time k . The knowledge of the probability distribution allows the user to formulate inequality constraints $g(\mathbf{x}[k]) \geq 0$ as chance constraints:

$$\Pr \{g(\mathbf{x}[k]) \geq 0\} \geq \beta \quad (18)$$

Here, $g(\cdot)$ is the inner constraint, and β is the probability value that should hold for satisfying the constraint. The function g might be nonlinear, and there exists no closed-form expression to implement Equation (18) into a numeric program. Instead, the chance constraint in Equation (18) can be replaced with a constraint on the corresponding quantile of the distribution of the function g :

$$g(\mathbf{x}[k])_{1-\beta} \geq 0 \quad (19)$$

In practice, the quantile $g(\mathbf{x}[k])_{1-\beta}$ is computed as an empirical quantile from evaluating g for every scenario computed in the propagation schemes presented in Section 2.2, i.e., the states' probability distribution is propagated through the inner constraint via Monte Carlo sampling. Note that the discrete-time formulation does not guarantee satisfying path constraints.

4 Simulation and dynamic optimization of a CSTR

This section applies the normalizing flow to learn the discrete time behavior of a CSTR and optimize the controls in an open-loop control setting. First, Section 4.1 introduces the case study. Next, Section 4.3 explains the training setup details and

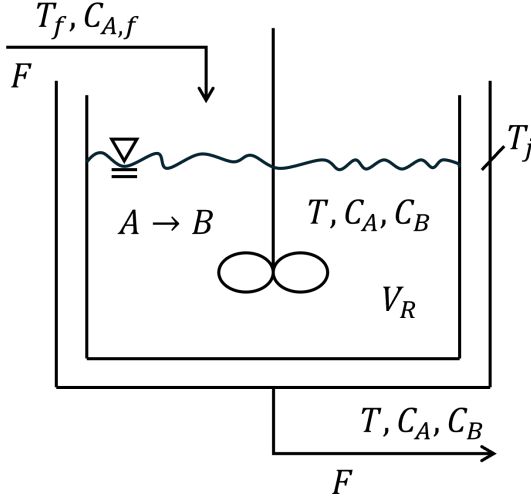


Fig. 2. Continuously stirred tank reactor (CSTR) sketch similar to [Bequette \(1998\)](#). State variables are the concentration of component A, $C_A(t)$, and the reactor temperature T . Control variables are the feed temperature T_f , the jacket temperature T_j , and the feed concentration of component A, $C_{A,f}$.

shows a probabilistic CSTR simulation. Finally, Section 4.4 shows the results of an open-loop MPC optimization using the normalizing flow model. The section further compares the results obtained from using either the stochastic or the probabilistic objective.

4.1 CSTR case study

The first case study in this work is the CSTR reactor model by [Bequette \(1998\)](#). The CSTR has two differential states: the reactor temperature T and the concentration C_A of the reagent A. The two states are controlled via three control inputs: the feed temperature T_f , the reactor jacket temperature T_j , and the concentration of the reagent A in the feed $C_{A,f}$. Equation System (20) shows the full model equations.

$$\begin{aligned} \frac{dC_A}{dt} &= \frac{F}{V_R} (C_{A,f} - C_A) - r \\ \frac{dT}{dt} &= \frac{F}{V_R} (T_f - T) - \frac{\Delta H}{\rho C_P} r - \frac{UA}{\rho C_P V_R} (T - T_j) \\ r &= k_0 C_A \exp\left(-\frac{E}{RT}\right) \end{aligned} \quad (20)$$

In Equation System (20), C_A is the concentration of component A, T is the reactor temperature, T_f is the feed temperature, T_j is the jacket temperature,

and $C_{A,f}$ is the feed concentration of component A. Figure 2 shows a sketch of the process. Table 1 lists the parameters and their values. The control variables and their limits are listed in Table 2.

4.2 Stochastic Process

Equation System (20) shows the nominal model. For the experiments in this work, the CSTR is studied as a stochastic process, i.e., random events impact the dynamics of the process. Such stochastic processes are common in bio-based processes such as cell growth or fermentation ([Álvarez et al., 2018](#)). To simulate data of the stochastic process, the ODE system is solved stepwise in 5-minute intervals. For each step, the realization is sampled from a Gaussian distribution. Specifically, the reaction term is set to be stochastic, which is described by sampling the concentration values as follows:

$$C_A[k] \sim \mathcal{N}(\bar{C}_A[k], \alpha \bar{C}_A[k] \Delta t) \quad (21)$$

Here, $\bar{C}_A[k]$ is the nominal simulation, α is a constant set to 1/3, and Δt is the 5-minute interval. Notably, the variance depends on the concentration, making the stochastic fluctuations state-dependent. The dynamics of the temperature are not stochastic. However, the stochastics of the concentration affect the dynamics of the temperature. In addition to the stochastic reaction, a 1% noise is added to the process data.

4.3 Simulation of CSTR behavior

The CSTR model is simulated with a discretization of 5 minutes per interval to create a dataset to train the normalizing flow. For the simulation, control inputs are randomly sampled from a uniform distribution over the control limits listed in Table 2. During the simulation, the control inputs are kept constant for 50 minutes, i.e., ten steps, for 1000 intervals. After simulation, the two states are normalized, and the controls are scaled to $[-1, 1]$ with -1 and 1 representing the maximum and minimum control actions in Table 2, respectively. The targets for the normalizing flow regression are created by shifting the simulation results by one step. The RealNVP ([Dinh et al., 2017](#)) normalizing flow is implemented using the python-based machine learning library *TensorFlow* ([Abadi and Agarwal, 2015](#)) and trained for 100 epochs using the optimizer Adam ([Kingma and Ba, 2015](#)) and a learning rate of 5×10^{-4} .

Figure 3 shows a simulation of the CSTR for ten 1 h intervals (12 time steps each) for randomly se-

Tab. 1. CSTR (Bequette, 1998) parameters from MathWorks (2024).

Parameter	Value	Unit	Description
F	1	m^3/h	Volumetric flow rate
V_R	1	m^3	Reactor volume
R	1.985	$\text{kcal}/(\text{kmol}\cdot\text{K})$	Ideal gas constant
ΔH	-5,96	kcal/kmol	Heat of reaction per mole
E	11,843	kcal/kmol	Activation energy per mole
k_0	34,930,800	1/h	Pre-exponential nonthermal factor
ρC_P	500	$\text{kcal}/(\text{m}^3\cdot\text{K})$	Density multiplied by heat capacity
UA	150	$\text{kcal}/(\text{K}\cdot\text{h})$	Overall heat transfer coefficient multiplied by tank area

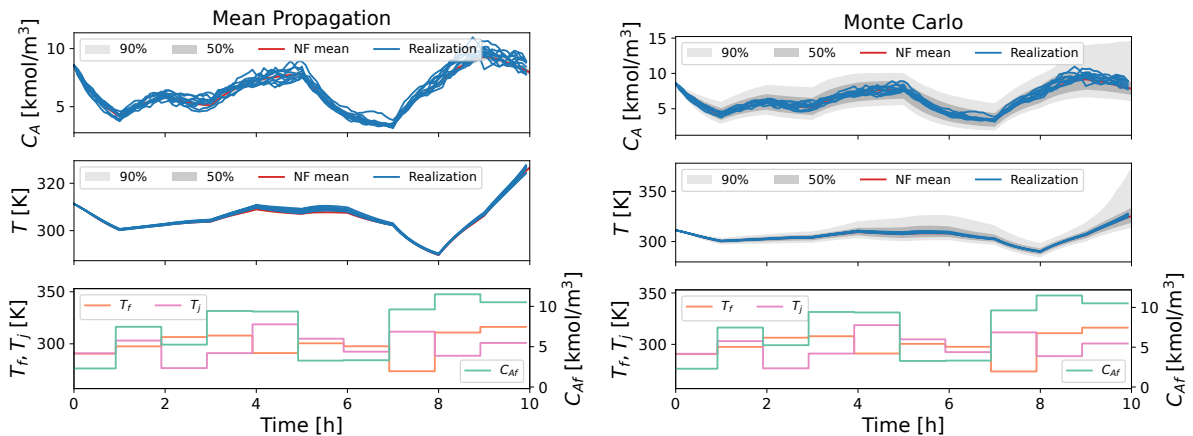


Fig. 3. Simulation of the reactor temperature T and the reagent concentration C_A for random control inputs. The first and the second rows show the mean (“NF mean”) and 50% and 90% prediction intervals for the normalizing flow in comparison to a simulation using the true model equations in (20) (“Realization”). The third row shows the randomly sampled control inputs. The left and right figures show the results for the “Mean Propagation” and the “Monte Carlo” simulation, respectively.

Tab. 2. CSTR control limits (Bequette, 1998).

	Min	Max
T_J [K]	273	322
T_f [K]	273	322
C_{Af} [kmol/m ³]	0	12

lected control values. The Figure shows the empirical mean values estimated by the normalizing flow, the 50% and 90% prediction intervals, and ten realization scenarios computed via the stochastic simulation of Equation System (20). The results in the left plot are computed using the mean value propagation, and the results in the right plot are computed using the Monte Carlo simulation. Both simulations only receive the initial values and the controls.

For both simulation approaches, the normalizing flow tracks the behavior of the reactor states well for both the reagent concentration C_A and reactor temperature T . For the Monte Carlo Simulation, the realization scenarios lie within the 50% prediction interval and generally fluctuate around the predicted empirical mean for the full 10 h simulation. The width of the prediction intervals increases over the length of the simulation, which is expected due to the increasing uncertainty resulting from the concentration's stochastic dynamics. Still, the simulation remains stable for all 120 simulated steps. For the mean value propagation, the prediction intervals remain narrow, and the realization scenarios frequently violate the prediction intervals. Still, the mean value propagation simulation remains stable throughout the simulation horizon.

The simulation in Figure 3 shows that the normalizing flow learns the dynamics of the CSTR well and also represents the stochastic dynamics of the concentration. Even for long simulation horizons with many consecutive evaluations, the normalizing flow gives reliable predictions of the process behavior and its probability distribution. The positive results in the simulation indicate good applicability for MPC applications with long prediction horizons.

4.4 Open-loop MPC

This section applies the normalizing flow model trained in Section 4.3 for open-loop MPC of the stochastic CSTR case study. The open-loop MPC solves the optimization of the stochastic formulation in Equation (15) and the maximum likelihood formulation in Equation (17) for a fixed time hori-

Tab. 3. Setpoints for open-loop control. Each setpoint is held for 2 h, which is 24 control intervals of 5 minutes each.

Setpoints	1	2	3	4
T [K]	301	308	290	320
C_A [kmol/m ³]	5.5	8	4.3	7

zon, respectively. Furthermore, the open-loop MPC is solved for both the mean value propagation and the Monte Carlo simulation for uncertainty propagation. In every time step, the stochastic formulation is solved for 1000 scenarios, and the Monte Carlo simulations are performed using 1000 scenarios. The controller aims to achieve four different setpoints after each other. The four setpoints are each held for 2 h, which equals 24 time steps in the discretization to 5 minutes. The optimizer may freely manipulate the three controls for every time step within the bounds listed in Table 2. The four setpoints are listed in Table 3.

The MPC optimization is solved in the scaled dataspace to match the outputs of the normalizing flow. Thus, the setpoints are scaled using the same scaling parameters from standardizing the training data. The data for the control inputs is scaled to the $[-1, 1]$ interval, with the extremes representing the control minimum and maximum controls, respectively. Thus, the bounds for the decision variables are set to -1 and 1 , respectively. Both the stochastic and probabilistic setpoint-tracking objective formulations are solved via the automatic differentiation wrapper in *autograd-minimize* (Rigal, 2023) and the python-based optimization library *scipy-optimize* (Virtanen et al., 2020).

The results are compared to a benchmark open-loop controller that optimizes over Equation System (20) directly without any interference from noise. Again, the control objective is formulated in the scaled space for a leveled comparison with the normalizing flow-based results. The objective for the benchmark reads:

$$\min_{\forall \mathbf{u}[k]} \sum_{t=1}^{N_T} (\hat{\mathbf{x}}^*[k] - \hat{\mathbf{x}}[k])^2 \quad (22)$$

Here, $\hat{\mathbf{x}}^*[k]$ and $\hat{\mathbf{x}}[k]$ are the scaled setpoints and states predicted by Equation System (20), respectively. The benchmark optimization problem is solved using the python-based optimization library *scipy-optimize* (Virtanen et al., 2020). Figure 4 shows the results of the benchmark optimization problem. The system is simulated ten times to

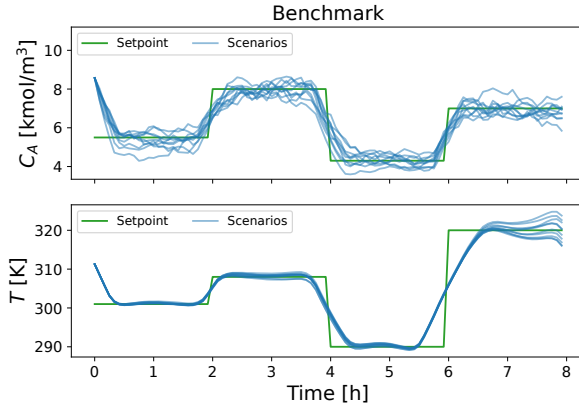


Fig. 4. Comparison of optimization results for the reactor temperature T and the reagent concentration C_A . The plots show realization scenarios of the process behavior with controls computed via the nominal open-loop MPC using Equation System (20).

obtain scenarios of the open-loop behavior. The benchmark simulation in Figure 4 shows good matches of the selected setpoints, which is expected as the optimization is solved using the equation system directly and without any noise.

Figure 5 shows realization scenarios for the control inputs computed via the four different combinations of stochastic (“Stochastic MPC”) objectives in Equation (14) and probabilistic (“Max Likelihood MPC”) objectives in Equation (17) as well as mean value propagation (“Mean Propagation”) and Monte Carlo simulation (“Monte Carlo”) in comparison to the setpoints. Overall, all solutions lead to good results for tracking the selected setpoints. There are slight overshoots for the concentration in the probabilistic objective with mean value propagation case, e.g., for the fourth setpoint. For the probabilistic objective with Monte Carlo simulation, the process deviates after the first hour of the fourth interval. Here, the Monte Carlo samples appear to deviate from the true process behavior, leading to a result drift. Both cases using the stochastic objective yield stable process behavior throughout the four setpoint periods.

Deviations such as the drift observed for the probabilistic objective with Monte Carlo samples appear only for longer horizons. In general, the control horizon for the open-loop study is long. In a closed-loop setting, only the first couple of steps would be implemented before the optimization is resolved with new measurements of the system’s states. The simulations for the first couple of time steps for the

normalizing flow approaches are almost identical to the benchmark solution. Hence, the results in Figure 5 indicate good performance for shorter time scales and good applicability for closed-loop control.

In summary, the normalizing flow learns the dynamics of the CSTR well and leads to good results in the MPC optimization. Overall, there appears to be no advantage to using either the maximum likelihood formulation or the stochastic scenario-based formulation.

5 Chance-constrained reactor cascade startup

This section presents the chance-constrained startup optimization of a reactor cascade. The goal of this dynamic program is to ramp up the product concentration at the outlet of the second of two reactors $C_{B,2}$ to be above $0.5 \frac{\text{kmol}}{\text{m}^3}$. First, Section 5.1 introduces the reactor cascade case study. Second, Section 5.2 shows the results of the chance-constrained startup optimization.

5.1 Reactor cascade

This section adapts the reactor cascade by Li (2007) to a dynamic process. The dynamic model consists of four component mass balances, one for every reactor and components A and B , respectively. Figure 6 shows a sketch of the two-reactor cascade. The component mass balances for each reactor $r \in \{1, 2\}$ are:

$$\begin{aligned} \frac{dC_{A,r}}{dt} &= \frac{F}{V_r} (C_{A,r-1} - C_{A,r}) - k_{A,r} C_{A,r} \\ \frac{dC_{B,r}}{dt} &= \frac{F}{V_r} (C_{B,r-1} - C_{B,r}) + k_{A,r} C_{A,r} V_r \\ &\quad - k_{B,r} C_{B,r} V_1 \end{aligned} \quad (23)$$

The reaction rates for components $c \in \{A, B\}$ are given by the Arrhenius equation:

$$k_{c,r} = k_{c,0} \cdot \exp\left(-\frac{E_c}{R \cdot T_r}\right) \quad (24)$$

Table 4 lists the kinetic parameter values. Operational costs are considered through an exponential term dependent on the temperature and the feed reactant concentration $C_{A,0}$. The combined objective function then is:

$$\min_{T_r} \sum_{t=1}^T \left(\exp(C_{A,0}[t]) + \sum_{r=1}^2 \exp\left(\frac{T_r[t]}{1000}\right) \right) \quad (25)$$

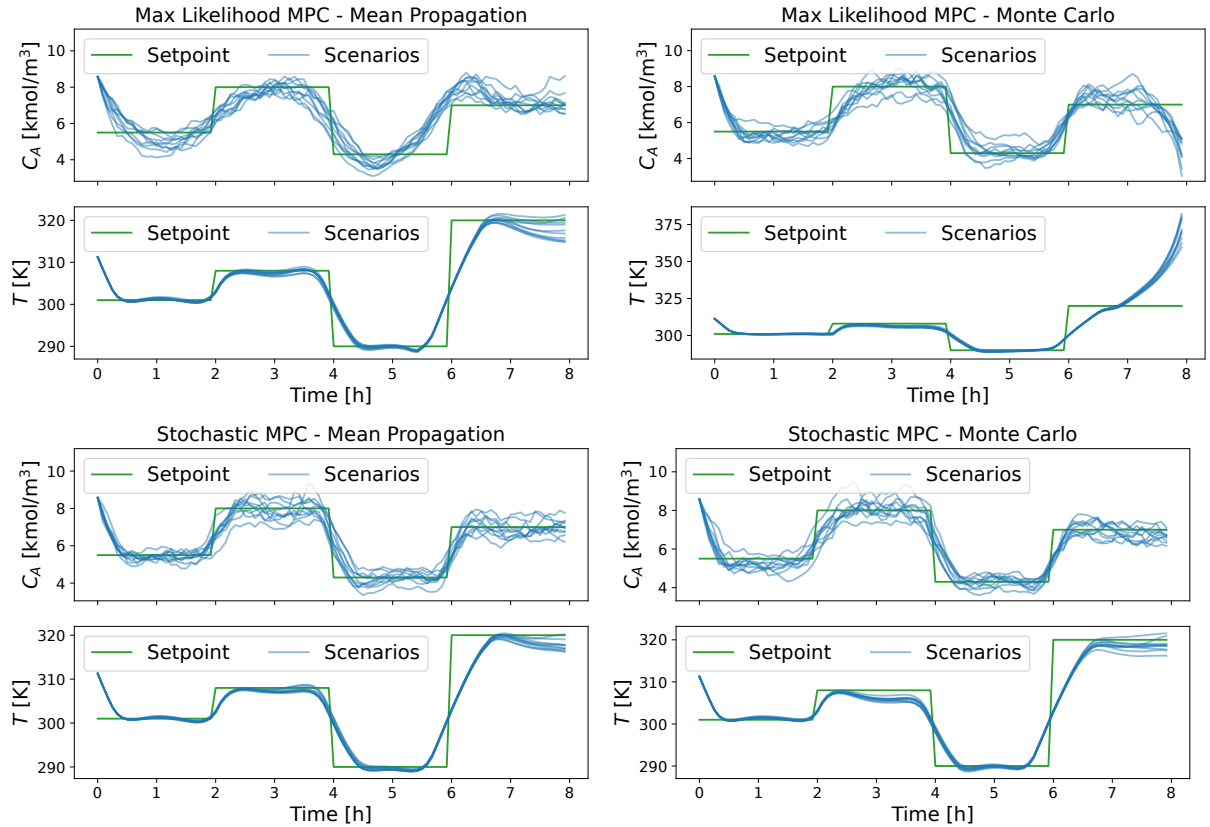


Fig. 5. Comparison of optimization results for the reactor temperature T and the reagent concentration C_A . The plots show simulations of the process behavior with controls computed via open-loop MPC for the stochastic objective formulation in Equation (14) (“Stochastic MPC”) and the likelihood objective formulation in Equation (17) (“Max Likelihood MPC”) in comparison to the setpoints (“Setpoints”).

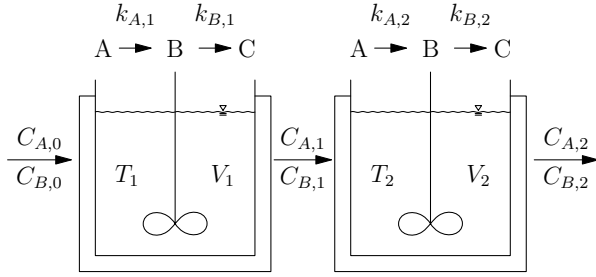


Fig. 6. Sketch of reactor cascade of two reactors. Feed: reactant A, Product: B, Byproduct: C. Similar to (Li, 2007).

Tab. 4. Kinetic parameters in reactor cascade.

$k_{A,0}$ [1/s]	$k_{B,0}$ [1/s]	E_A [J]	E_B [J]
0.715	0.182	6665.948	7965.248

To keep the process profitable, the output concentration of the product B of the second reactor has to be greater or equal to 0.5 after a startup period of four hours:

$$c_{B,2}(t \geq 4 \text{ h}) \geq 0.5 \frac{\text{kmol}}{\text{m}^3} \quad (26)$$

The feed does not contain any product $c_{B,0} = 0$, the constant feed flow is $F = 1 \text{ m}^3/\text{s}$, and the reactor volumes are $V_r = 2.5 \text{ m}^3$ each. Table 5 lists the control limits for the reactor cascade.

Again, the process is studied as a stochastic process, and the process data is simulated using the sampling approach described in Section 4.2. The probability of achieving the desired product quality for times greater than 4 h should be 90%. Hence, Equation (26) can be reformulated as a chance constraint:

$$\Pr \left\{ C_{B,2}(t \geq 4 \text{ h}) - 0.5 \frac{\text{kmol}}{\text{m}^3} \geq 0 \right\} \geq 0.9 \quad (27)$$

5.2 Startup optimization using normalizing flows

The dynamic system in Equation (23) is described via the DTM formulation using normalizing flows

Tab. 5. Reactor cascade control limits (Li, 2007).

	Min	Max
T_1 [K]	273	1000
T_2 [K]	273	1000
$C_{A,0}$ [kmol/m ³]	0	3

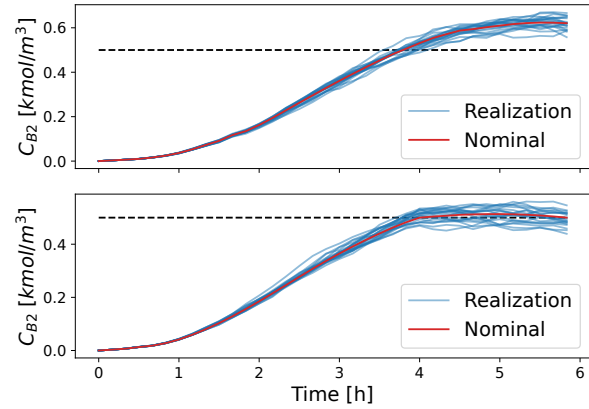


Fig. 7. Start-up optimization of reactor cascade to achieve $c_{B,2}(t \geq 4 \text{ h}) \geq 0.5 \frac{\text{kmol}}{\text{m}^3}$. Top: Simulation of process startup with results from normalizing flow-based optimization. Bottom: Simulation of process startup with results from nominal optimization. The dashed line represents the $0.5 \frac{\text{kmol}}{\text{m}^3}$ threshold.

described in Section 2. The chance-constrained program is formulated via the empirical quantile approach described in Section 3.3, and the simulation uses the particle swarm approach described in Section 2.2. The process is considered in $\Delta t = 10 \text{ min}$ time intervals, and the stochastic factor α in Equation (21) is set to 0.1. Furthermore, there is a 3% measurement noise added to the simulations.

Figure 7 shows 20 simulations of the first six hours of the product concentration $C_{B,2}$ for normalizing flow-based chance-constrained optimization (top) and nominal optimization using the process model in Equation (23) (bottom), respectively. The startup schedule obtained using the normalizing flow-based optimization shows a minimal violation of the constraint for a few of the simulations 4 h into the startup. For times greater than 4 h, there are no violations of the constraint. For the nominal solution, however, about half of the simulations of the stochastic reactor cascade show violations of the constraints for times $\geq 4 \text{ h}$. These violations are expected as the nominal problem does not reflect the stochastic nature of the reactions.

In summary, the normalizing flow-based chance-constrained formulation achieves a feasible startup schedule for the reactor cascade.

6 Conclusion

This work applies the deep generative model called normalizing flows as a probabilistic DTM for chemical processes. The conditional PDF formulation of normalizing flows learns both the discrete-time dynamics and stochastics with high flexibility, as there are no prior assumptions about the process's dynamics or probability distribution.

Applying the normalizing flow DTM to a CSTR case study shows stable simulations for long time horizons with varying control inputs. Furthermore, the normalizing flow yields good results in the open-loop MPC. Only for long time horizons does the open-loop control diverge from the setpoints. This work further compares stochastic and probabilistic formulations of the MPC objective. The open-loop control results show similar results for both formulations, i.e., the investigation in this study shows no advantage of using either formulation over the other. The reactor cascade case study highlights how normalizing flow-based DTM models can be used to formulate chance constraints that achieve feasible and reliable startup schedules for reactors with stochastic reactions.

In conclusion, normalizing flows present a versatile tool for learning probabilistic DTM of chemical processes. They learn stochastic dynamics from process data and allow for stochastic and probabilistic MPC formulations. Furthermore, the empirical quantile-based chance constraint formulation achieves reliable results.

Future work will investigate closed-loop control based on normalizing flow process models and the real-time applicability of such a controller. Furthermore, processes with more exotic types of noise, such as multimodal distributions, will be investigated.

Bibliography

Abadi, M. and Agarwal, A. (2015). TensorFlow: Large-scale machine learning on heterogeneous systems. <https://www.tensorflow.org/>. Accessed on 08-08-2022.

Bequette, B. W. (1998). Process dynamics: modeling, analysis, and simulation. Lecture notes.

Birge, J. R. and Louveaux, F. (2011). *Introduction to stochastic programming*. Springer Science & Business Media, New York, US.

Box, G. E., Jenkins, G. M., and Bacon, D. W. (1967). Models for forecasting seasonal and non-seasonal time series. Technical report, Wisconsin Univ. Madison Department of Statistics.

Cramer, E., Mitsos, A., Tempone, R., and Dahmen, M. (2022a). Principal component density estimation for scenario generation using normalizing flows. *Data-Centric Engineering*, 3:e7.

Cramer, E., Paeleke, L., Mitsos, A., and Dahmen, M. (2022b). Normalizing flow-based day-ahead wind power scenario generation for profitable and reliable delivery commitments by wind farm operators. *Computers & Chemical Engineering*, 166:107923.

Cramer, E., Witthaut, D., Mitsos, A., and Dahmen, M. (2023). Multivariate probabilistic forecasting of intraday electricity prices using normalizing flows. *Applied Energy*, 346:121370.

Dinh, L., Krueger, D., and Bengio, Y. (2015). NICE: Non-linear independent components estimation. In Bengio, Y. and LeCun, Y., editors, *3rd International Conference on Learning Representations, ICLR 2015, San Diego, CA, USA, May 7-9, 2015, Workshop Track Proceedings*.

Dinh, L., Sohl-Dickstein, J., and Bengio, S. (2017). Density estimation using Real NVP. In *5th International Conference on Learning Representations, ICLR 2017, Toulon, France, April 24-26, 2017, Conference Track Proceedings*. Open-Review.net.

Grathwohl, W., Chen, R. T. Q., Bettencourt, J., Sutskever, I., and Duvenaud, D. (2018). FFJORD: free-form continuous dynamics for scalable reversible generative models. *CoRR*, abs/1810.01367.

Hilger, H., Witthaut, D., Dahmen, M., Rydin Gorjão, L., Trebbien, J., and Cramer, E. (2024). Multivariate scenario generation of day-ahead electricity prices using normalizing flows. *Applied Energy*, 367:123241.

Kingma, D. P. and Ba, J. (2015). Adam: A method for stochastic optimization. In Bengio, Y. and LeCun, Y., editors, *3rd International Conference on Learning Representations, ICLR 2015, San Diego, CA, USA, May 7-9, 2015, Conference Track Proceedings*, pages 1–11.

Li, P. (2007). *Prozessoptimierung unter Unsicherheiten*. OLDENBOURG WISSENSCHAFTSVERLAG.

MathWorks (2024). Time series. <https://de.mathworks.com/help/mpc/gs/cstr-model.html>. Accessed: 2024-04-23.

Mesbah, A. (2016). Stochastic model predictive control: An overview and perspectives for future research. *IEEE Control Systems*, 36(6):30–44.

Mesbah, A., Wabersich, K. P., Schoellig, A. P., Zeilinger, M. N., Lucia, S., Badgwell, T. A., and Paulson, J. A. (2022). Fusion of machine learning and mpc under uncertainty: What advances are on the horizon? In *2022 American Control Conference (ACC)*. IEEE.

Papamakarios, G., Nalisnick, E., Rezende, D. J., Mohamed, S., and Lakshminarayanan, B. (2021). Normalizing flows for probabilistic modeling and inference. *Journal of Machine Learning Research*, 22(57):1–64.

Paulson, J. A., Buehler, E. A., Braatz, R. D., and Mesbah, A. (2017). Stochastic model predictive control with joint chance constraints. *International Journal of Control*, 93(1):126–139.

Rasul, K., Sheikh, A.-S., Schuster, I., Bergmann, U. M., and Vollgraf, R. (2021). Multivariate probabilistic time series forecasting via conditioned normalizing flows. In *International Conference on Learning Representations*, Vienna, Austria.

Rawlings, J. B., Mayne, D. Q., Diehl, M., et al. (2017). *Model predictive control: theory, computation, and design*, volume 2. Nob Hill Publishing Madison, WI.

Ren, Y. M., Alhajeri, M. S., Luo, J., Chen, S., Abdulla, F., Wu, Z., and Christofides, P. D. (2022). A tutorial review of neural network modeling approaches for model predictive control. *Computers & Chemical Engineering*, 165:107956.

Rigal, B. (2023). autograd-minimize. <https://github.com/brunorigal/autograd-minimize>.

Rossi, R. J. (2018). *Mathematical statistics: An introduction to likelihood based inference*. John Wiley & Sons.

Schwarm, A. T. and Nikolaou, M. (1999). Chance-constrained model predictive control. *AIChE Journal*, 45(8):1743–1752.

Söderström, T. (2002). *Discrete-time Stochastic Systems: Estimation and Control*. Springer London.

Tan, W. G. Y. and Wu, Z. (2024). Robust machine learning modeling for predictive control using lipschitz-constrained neural networks. *Computers & Chemical Engineering*, 180:108466.

Varshney, D., Patwardhan, S. C., Bhushan, M., and Biegler, L. T. (2022). Moving horizon estimator for nonlinear and non-gaussian stochastic disturbances. *Journal of Process Control*, 116:234–254.

Virtanen, P., Gommers, R., Oliphant, T. E., Haberland, M., Reddy, T., Cournapeau, D., Burovski, E., Peterson, P., Weckesser, W., Bright, J., van der Walt, S. J., Brett, M., Wilson, J., Millman, K. J., Mayorov, N., Nelson, A. R. J., Jones, E., Kern, R., Larson, E., Carey, C. J., Polat, İ., Feng, Y., Moore, E. W., VanderPlas, J., Laxalde, D., Perktold, J., Cimrman, R., Henriksen, I., Quintero, E. A., Harris, C. R., Archibald, A. M., Ribeiro, A. H., Pedregosa, F., van Mulbregt, P., and SciPy 1.0 Contributors (2020). SciPy 1.0: Fundamental Algorithms for Scientific Computing in Python. *Nature Methods*, 17:261–272.

Winkler, C., Worrall, D., Hoogeboom, E., and Welling, M. (2019). Learning likelihoods with conditional normalizing flows. *arXiv preprint arXiv:1912.00042*.

Wu, Z., Rincon, D., and Christofides, P. D. (2020). Process structure-based recurrent neural network modeling for model predictive control of nonlinear processes. *Journal of Process Control*, 89:74–84.

Zheng, Y., Hu, C., Wang, X., and Wu, Z. (2023). Physics-informed recurrent neural network modeling for predictive control of nonlinear processes. *Journal of Process Control*, 128:103005.

Álvarez, J., Baratti, R., Tronci, S., Grosso, M., and Schaum, A. (2018). Global-nonlinear stochastic dynamics of a class of two-state two-parameter non-isothermal continuous stirred tank reactors. *Journal of Process Control*, 72:1–16.